

Article

Magnetron Sputter-Deposited β -Ga₂O₃ Films on c-Sapphire Substrate: Effect of Rapid Thermal Annealing Temperature on Crystalline Quality

Sakal Pech [†], Sara Kim [†]  and Nam-Hoon Kim ^{*} 

Department of Electrical Engineering, Chosun University, Gwangju 61452, Korea; pechsakal@chosun.kr (S.P.); sarakim@chosun.kr (S.K.)

^{*} Correspondence: nhkim@chosun.ac.kr; Tel./Fax: +82-62-230-7028[†] These authors contributed equally to this work.

Abstract: Gallium oxide (Ga₂O₃) is a semiconductor with a wide bandgap of ~5.0 eV and large breakdown voltages (>8 MV·cm⁻¹). Among the crystal phases of Ga₂O₃, the monoclinic β -Ga₂O₃ is well known to be suitable for many device applications because of its chemical and thermal stability. The crystalline quality of polycrystalline β -Ga₂O₃ films on c-plane sapphire substrates was studied by rapid thermal annealing (RTA) following magnetron sputtering deposition at room temperature. Polycrystalline β -Ga₂O₃ films are relatively simple to prepare; however, their crystalline quality needs enhancement. The β -phase was achieved at 900 °C with a crystallite size and *d*-spacing of 26.02 and 0.2350 nm, respectively, when a mixture of ϵ - and β -phases was observed at temperatures up to 800 °C. The strain was released in the annealed Ga₂O₃ films at 900 °C; however, the clear and uniform orientation was not perfect because of the increased oxygen vacancy in the film at that temperature. The improved polycrystalline β -Ga₂O₃ films with dominant (−402)-oriented crystals were obtained at 900 °C for 45 min under a N₂ gas atmosphere.



Citation: Pech, S.; Kim, S.; Kim, N.-H. Magnetron Sputter-Deposited β -Ga₂O₃ Films on c-Sapphire Substrate: Effect of Rapid Thermal Annealing Temperature on Crystalline Quality. *Coatings* **2022**, *12*, 140. <https://doi.org/10.3390/coatings12020140>

Academic Editor: Gianni Barucca

Received: 27 December 2021

Accepted: 23 January 2022

Published: 25 January 2022

Publisher's Note: MDPI stays neutral with regard to jurisdictional claims in published maps and institutional affiliations.



Copyright: © 2022 by the authors. Licensee MDPI, Basel, Switzerland. This article is an open access article distributed under the terms and conditions of the Creative Commons Attribution (CC BY) license (<https://creativecommons.org/licenses/by/4.0/>).

Keywords: β -Ga₂O₃; magnetron sputtering; c-sapphire substrate; rapid thermal annealing

1. Introduction

Gallium oxide (Ga₂O₃) is a semiconductive material with a direct bandgap of 4.5–5.0 eV, remarkable thermal and chemical stability, high transparency in ultraviolet (UV) and visible (VIS) regions, and high dielectric constants in the range of 10.2–14.2 [1]. The monoclinic β -Ga₂O₃ is more stable than the α -, γ -, δ -, and ϵ -phases with n-type conductivity owing to oxygen vacancy as a donor level [2]. The other four phases are metastable and can transform to β -Ga₂O₃ at temperatures above 750 °C [1,3]. β -Ga₂O₃ has attracted attention for future electronic applications, owing to its distinguished properties, such as an ultra-wide bandgap range of 4.7–4.9 eV, a critical electric field (E_C) strength of 8 MV/cm, an excellent electron mobility of 300 cm²/V·s, and an exceptional Baliga figure of merit (BFOM) of 3444 [1,4].

Polycrystalline β -Ga₂O₃ films are relatively simple to prepare; however, their poor crystalline quality does not meet the requirements for certain electronic applications. Conversely, the preparation of single-crystal β -Ga₂O₃ with high crystalline quality is complicated and costly. β -Ga₂O₃ films with highly preferred orientation can offer suitable crystalline quality between single crystal and polycrystalline, showing a balance between physical properties and cost [5]. Many efforts have been made by relevant technologies to achieve high crystalline quality polycrystalline β -Ga₂O₃ films [1,2]; however, suitable substrate is required to prevent a large lattice mismatch and coordination difference at the interface between the films and substrate [6,7].

Notably, various substrates such as sapphire (Al₂O₃), magnesium oxide (MgO), yttria-stabilized zirconia (YSZ), gallium arsenide (GaAs), and Si have been employed for the

heteroepitaxy of β -Ga₂O₃ [8,9]. In particular, the c-plane (0001) sapphire has been widely employed as a substrate for β -Ga₂O₃ because of its six-fold symmetry. Crystals of (−201)-oriented β -Ga₂O₃ also exhibit six-fold symmetry and similar thermal expansion coefficients as β -Ga₂O₃ ($\alpha_c = 3.15 \times 10^{-6} \text{ K}^{-1}$) and sapphire ($\alpha_c = \sim 4.3 \times 10^{-6} \text{ K}^{-1}$) [6,10].

For the heteroepitaxy of β -Ga₂O₃, dislocations are created inside the epitaxy layer to relax the residual stress, degrading the performance of the devices [11]. A buffer layer between the c-plane sapphire substrate and the epitaxy layer can be a solution to reduce the difference in the lattice constants to decrease the residual stress [12–14]. In α -Ga₂O₃ epitaxial growth, the buffer layer using some metal alloys decreased threading dislocation density significantly and eliminated strain accumulation at the α -Ga₂O₃–sapphire interface [14–16]. Because β -Ga₂O₃ for power device applications requires significantly fewer defects than for optical device applications, to produce a high-quality monoclinic-phase β -Ga₂O₃ epitaxial layer for power device applications, high-quality polycrystalline β -Ga₂O₃ films on a c-plane sapphire substrate are proposed as the buffer layer, which acts as a lattice template in this study. Because the quality of the β -Ga₂O₃ homoepitaxial layer with fewer defects, such as threading dislocation and twin boundary, was determined according to the dislocation density of the substrate [17], it is necessary to focus on the crystalline quality of the β -Ga₂O₃ buffer layer.

Radio frequency (RF) magnetron sputtering deposition was selected to prepare high-quality polycrystalline β -Ga₂O₃ films on a c-plane sapphire substrate for industrial mass production among the various methods. The RF magnetron sputtering method can produce high-quality films with low cost, high deposition rate, easy control of process parameters, suitable uniformity, high homogeneity, and significant adhesion over a comparatively large area. Polycrystalline β -Ga₂O₃ films are universally obtained at elevated substrate temperatures during film deposition because β -Ga₂O₃ crystallization can only be realized at relatively high temperatures [18]. Another method is to fabricate polycrystalline β -Ga₂O₃ films through a two-step method by post-annealing the as-deposited Ga₂O₃ films at room temperature. Here, the β -Ga₂O₃ films were fabricated and characterized by post-annealing with a rapid thermal annealing (RTA) system at various temperatures after deposition onto c-plane sapphire substrates by RF magnetron sputtering at room temperature to enhance the crystalline quality. There have been several previous investigations on the effects of the post-annealing process of sputter-deposited Ga₂O₃ films [2,19,20], but there have been few studies to apply these films as a lattice template on the c-sapphire substrate for application to power devices, except for optical devices. For the fabrication of the β -Ga₂O₃ buffer layer at high temperatures, the residual stress of the β -Ga₂O₃ films should be studied intensively as a function of the temperature.

2. Experimental Details

Ga₂O₃ films were deposited on $1 \times 1 \text{ cm}^2$ c-plane (0001) sapphire substrates using an RF magnetron sputtering system (IDT Engineering Co., Gyeonggi, Korea) at room temperature [21], with a Ga₂O₃ (TASCO, Seoul, Korea, 99.999% purity, 5.08 cm diameter) target under a fixed set of process parameters: a pre-sputtering process for 5 min prior to each run, a frequency of 13.56 MHz, an RF sputtering of 100 W, an Ar gas flow rate of 50 sccm, a base pressure of $133.3224 \times 10^{-6} \text{ Pa}$, a substrate-to-target distance of 5.0 cm, and a vacuum pressure of $999.9178 \times 10^{-3} \text{ Pa}$ during sputtering at room temperature. The deposition time was fixed at 34 min to obtain a constant thickness of approximately 200 nm (Figure S1, in Supplementary Materials). After the sputtering deposition, the samples were subjected to RTA (GRT-100, GD-Tech Co., Gyeongsangbuk, Korea) from 500 to 900 °C for 45 min under a N₂ gas atmosphere [19,22].

The crystalline structure of the films was analyzed using X-ray diffraction (XRD, PANalytical B.V., Almelo, The Netherlands, X'pert-PRO-MRD, Cu K α = 0.15405 nm, 40 kV, 30 mA) over a 2θ range of 10–80° with a step size of 0.026° and scanning speed of 8.5°/min. Field emission scanning electron microscopy (FESEM, JEOL, Tokyo, Japan, JSM-7500F) was employed to reveal the morphological characteristics of the Ga₂O₃ films. X-ray photoelec-

tron spectroscopy (XPS, Thermo Fisher Scientific Inc., Waltham, MA, USA, K-Alpha⁺) was used to analyze the composition and chemical nature of the Ga₂O₃ films. Field emission transmission electron microscopy (FETEM, JEOL, Tokyo, Japan, JEM-2100F, a field emission gun source at 200 kV) and selected area electron diffraction (SAED) were performed to evaluate the quality of the crystal lattice.

3. Results and Discussion

The surface morphologies of the as-deposited and annealed Ga₂O₃ films at different post-annealing temperatures were analyzed using FESEM. Figure 1 shows the top-view FESEM images of the Ga₂O₃ films on the c-plane (0001) sapphire substrates. None of the as-deposited and annealed Ga₂O₃ films had extended cracks after the ex situ annealing process using the RTA system [23]. The as-deposited film showed that the surface morphologies comprised fine grains tightly connected with a relatively clear boundary, as shown in Figure 1a. There was no significant difference between the annealed film at 500 °C and the as-deposited films. For the annealed film at 600 °C, the high annealing temperature provided the as-deposited grains with thermal energy to accumulate to form large grains with blurred boundaries. Distorted hexagonal islands occurred on the surfaces of the annealed film at 700 °C, as shown in Figure 1d, similar to the reported island nucleation of ε-Ga₂O₃ in epitaxial growth on a c-plane sapphire substrate by metalorganic chemical vapor deposition at 650 °C [12,24,25]. It was considered that agglomeration, rather than the merging into large crystals, began to occur at 800 °C in a part of the film, and discontinuities and voids were observed [26]. Uniform, dense, compact, and well-defined grains with clear boundaries were observed in the annealed films at 900 °C; the grain size gradually increased with an increase in the annealing temperature from 500 to 900 °C.

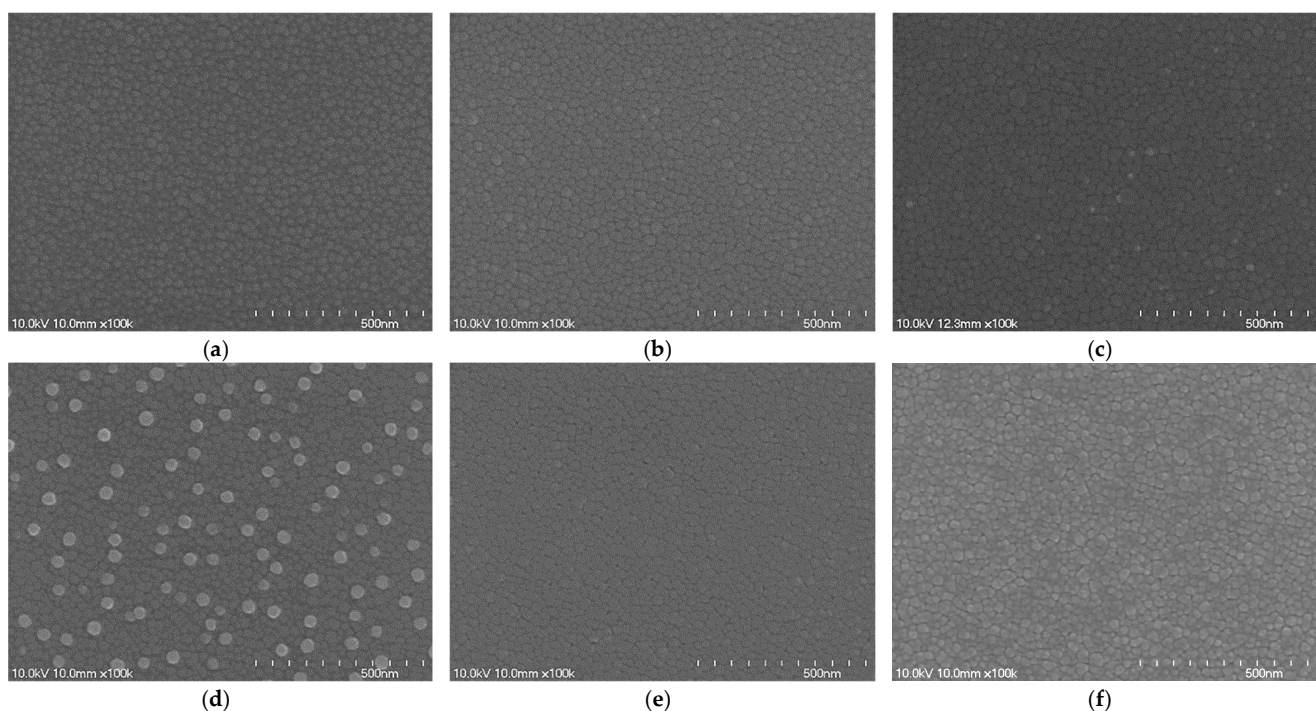


Figure 1. Top-view field emission scanning electron microscopy (FESEM) surface images of (a) as-deposited and annealed Ga₂O₃ films at different post-annealing temperatures: (b) 500, (c) 600, (d) 700, (e) 800, and (f) 900 °C.

The as-deposited Ga₂O₃ films exhibited amorphous or microcrystalline structures. A post-annealing process was performed by RTA to improve their crystallinity. Figure 2a shows the XRD patterns of the as-deposited and annealed Ga₂O₃ films at various annealing temperatures in the 2θ range of 10–80°. The XRD patterns of the annealed film at 500 °C

show broad amorphous features and weak peaks along with (006) and (003) diffraction peaks from the sapphire substrate, which indicates that the β - Ga_2O_3 crystallization was not easily achieved under the low annealing temperature of 500 °C. It was observed that three diffraction peaks along (−201), (−402), and (−603) at $2\theta = 18.38^\circ$, 38.21° , and 58.84° , respectively, corresponded to β - Ga_2O_3 at the annealing temperature of 600–900 °C (ICDD/JCPDS PDF card No. 87-1901). This reveals that the arrangement of oxygen atoms in the β - Ga_2O_3 (−201) plane was equivalent to that in the c-plane sapphire [27,28]. In contrast, the annealed Ga_2O_3 films at 600 and 700 °C comprised three diffraction peaks along (0002), (0004), and (0006) at $2\theta = 19.09^\circ$, 37.62° , and 59.12° , respectively, corresponding to ϵ - Ga_2O_3 . The shoulder of ϵ - Ga_2O_3 at the diffraction peak along (−402), corresponding to β - Ga_2O_3 at $2\theta = 38.12^\circ$, disappeared in the annealed Ga_2O_3 film at 800 °C, while a diffraction peak along (0002) remained at $2\theta = 19.10^\circ$, corresponding to ϵ - Ga_2O_3 . The metastable ϵ -phase transformed into the thermodynamically stable β -phase within the range of 700–800 °C [3,12,29,30]. The intensities of the diffraction peaks along (−201), (−402), and (−603) increased with an increase in temperature, as shown in Figure 2a.

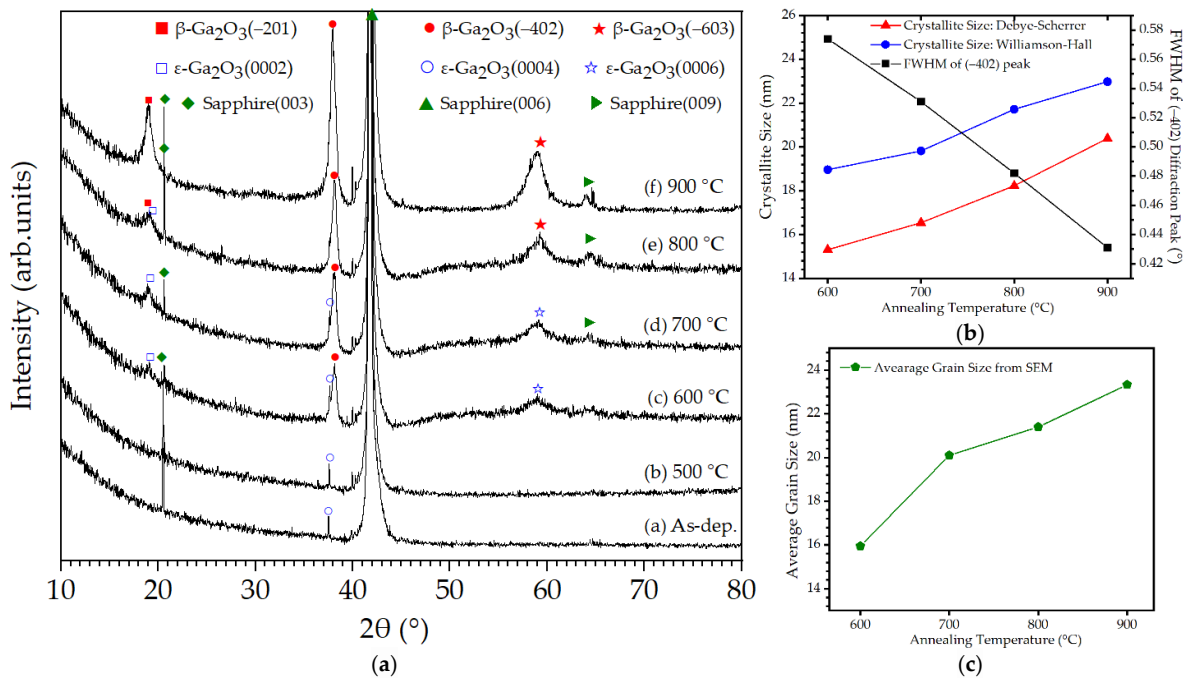


Figure 2. (a) X-ray diffraction (XRD) patterns of the as-deposited and annealed Ga_2O_3 films with different annealing temperatures of 500, 600, 700, 800, and 900 °C [31]. (b) Full widths at half maximum (FWHM) and crystallite size along the (−402) plane of the annealed Ga_2O_3 films with the annealing temperature from 600 to 900 °C. (c) Average grain sizes under the same conditions.

The full width at half maximum (FWHM) of the (−402) diffraction peak, as a function of the annealing temperature, is shown in Figure 2b. This FWHM decreased to 0.428° with an increase in temperature from 600 to 900 °C, which was attributed to the large driving energy to migrate atoms to suitable lattice sites to achieve high crystalline quality at 900 °C [32]. However, it was considered that certain stresses caused by internal/external factors affected the structure of the films at this temperature [33,34]. The crystallite size of the films was estimated from the (−402) diffraction peak using both the Debye–Scherrer formula $D_{D-S} = 0.94 \lambda / \omega \cdot \cos\theta$ and Williamson–Hall equation $D_{W-H} = 0.94 \lambda / (\omega \cdot \cos\theta - \epsilon \cdot \sin\theta)$ [35–38], where λ is the $K\alpha$ radiation wavelength of Cu ($\lambda = 0.15406$ nm), ω is the FWHM of the (−402) diffraction peak, ϵ is the lattice strain, and θ is the Bragg angle corresponding to the (−402) diffraction peak. The crystallite size gradually increased from 15.30 to 20.50 nm for D_{D-S} and 18.97 to 22.98 nm for D_{W-H} with an increase in temperature from 600 to 900 °C, as shown in Figure 2b. In comparison with D_{D-S} and D_{W-H} , the overall D_{W-H} exhibited large values, showing a similar tendency to

increase, while the slopes of the increase in D_{W-H} were relatively lower than those in D_{D-S} at 700 and 900 °C. In the Williamson–Hall equation, the Bragg angle of the diffraction peak along (−402) shifted toward lower values from $2\theta = 38.21^\circ$ to 37.98° with an increase in temperature from 600 to 900 °C. This shift was revealed as one of the main reasons for the larger values of D_{W-H} compared to those of D_{D-S} , although the effect of strain remains to be further investigated. According to Bragg’s law, the shift in the Bragg angle was affected by a change in the spacing of the crystallographic planes, where the tensile strain increases the d -spacing, causing a shift in the Bragg angle of the diffraction peak towards lower 2θ values, whereas compressive strain decreases the d -spacing, resulting the shift towards higher 2θ values in the XRD pattern [39]. Average grain size, which was estimated using SEM images and ImageJ software [40], is also shown in Figure 2c.

The diffraction data analysis with lattice constants (a , b , c , and β) was refined using X’Pert HighScore Plus software (Panalytical B.V., Almelo, The Netherlands) [41,42]. The lattice constants of the monoclinic β -Ga₂O₃ are generally $a = 1.223 \pm 0.002$ nm, $b = 0.304 \pm 0.001$ nm, and $c = 0.580 \pm 0.001$ nm, and the angle between the a - and c -axes is $\beta = 103.7 \pm 0.3^\circ$ [1,43,44]. Above 600 °C, the annealed film exhibited a typical monoclinic crystal structure with two inequivalent Ga sites and three inequivalent O sites. The lattice constants slightly changed with an increase in the annealing temperature from 600 to 900 °C, while the lattice constants of the Ga₂O₃ film at 600 °C were $a = 1.2219$ nm, $b = 0.3035$ nm, $c = 0.5803$ nm, and $\beta = 104.06^\circ$. There were slight fluctuations in the a value (1.2190–1.2220 nm) and c value (0.5803–0.5821 nm) when the b value varied between 0.3019 and 0.3035 nm. The β value showed a tendency to decrease from 104.06° at 600 °C to 103.86° at 800 °C and suddenly returned to 104.06° at 900 °C. This variation in the lattice constants is shown in Figure 3a–d with an increase in temperature, indicating that the lattice constants of the strained lattice of Ga₂O₃ are far from their bulk values. The volume of a unit cell was obtained from the expression for monoclinic systems: $V = abc \cdot \sin\beta$. The volumes of the unit cell in all annealed films were in the range of 208.70×10^{-3} – 208.83×10^{-3} nm³, which was less than the corresponding bulk value of 209.63×10^{-3} nm³ at all temperatures [8,33], as shown in Figure 3e, indicating that the Ga₂O₃ films compressively strained the unit cell of the films within the range of 600–900 °C. There are two distinct Ga sites: the Ga(I) atoms are bonded to four neighboring O atoms in a tetrahedral arrangement, while the Ga(II) atoms are octahedrally arranged and bound to six neighboring O atoms [44]. The wave function of the conduction band bottom generally comprises 4s orbitals of Ga³⁺ ions in octahedral sites [29]. A compressive strain may lead to an increased octahedral occupancy by Ga³⁺ ions, forming a compact structure in the unit cell, whereas a tensile strain in the film may lead to an influx of Ga³⁺ ions in the tetrahedral sites, forming a relatively loose structure [29].

Figure 3f shows the strain (ϵ) due to crystal imperfections and distortions of the Ga₂O₃ films that were annealed at 600, 700, 800, and 900 °C, as calculated using the equation $\epsilon = \omega/4\tan\theta$, where ω is the FWHM of the predominant diffraction peak and θ is the Bragg angle corresponding to the diffraction peak obtained from the XRD data [45–47]. The strains along the (−402) orientation decreased from a maximum of 8.562×10^{-3} at 600 °C to a minimum of 6.187×10^{-3} at 900 °C. With an increase in the annealing temperature from 600 to 900 °C and a relaxation in the compressive strain, an increasing number of Ga³⁺ ions occupied the oxygen tetrahedral sites from the oxygen octahedral sites; therefore, the volume of the unit cell showed the slightly volumetric contraction at 700 °C although the compressive strain released rapidly, while volumetric expansion occurred for compact structures at 800–900 °C as the compressive strain released, as shown in Figure 3e,f. The volumetric expansion and transformation of the ϵ -phase into the thermodynamically stable β -phase occurred at 800 °C [24,25,29]. The proportion of octahedrally and tetrahedrally coordinated Ga is 1:1 in the monoclinic β -phase when the disordered Ga atoms occupy octahedral and tetrahedral sites to give the 2:3 stoichiometry in the ϵ -phase [48]. It is suspected that volume expansion was limited at 900 °C as a relatively increased octahedral occupancy by Ga³⁺ ions due to the transformation from ϵ - to β -phase. The dislocation

density (δ) of the Ga_2O_3 films was calculated at the same annealing temperatures using the equation $\delta = 1/D^2$, where D is the crystallite size obtained from the XRD data. A similar trend in the dislocation density was obtained for the strain along the (-402) orientation (*not shown*). The lowest value of 2.3790×10^{15} line/m² along the (-402) orientation was obtained at 900 °C when the dislocation density decreased from the highest value of 4.2730×10^{15} line/m² at 600 °C. This indicates that the largest crystallite size (Figure 2b) was observed at 900 °C as a result of the released compressive strain and dislocation density.

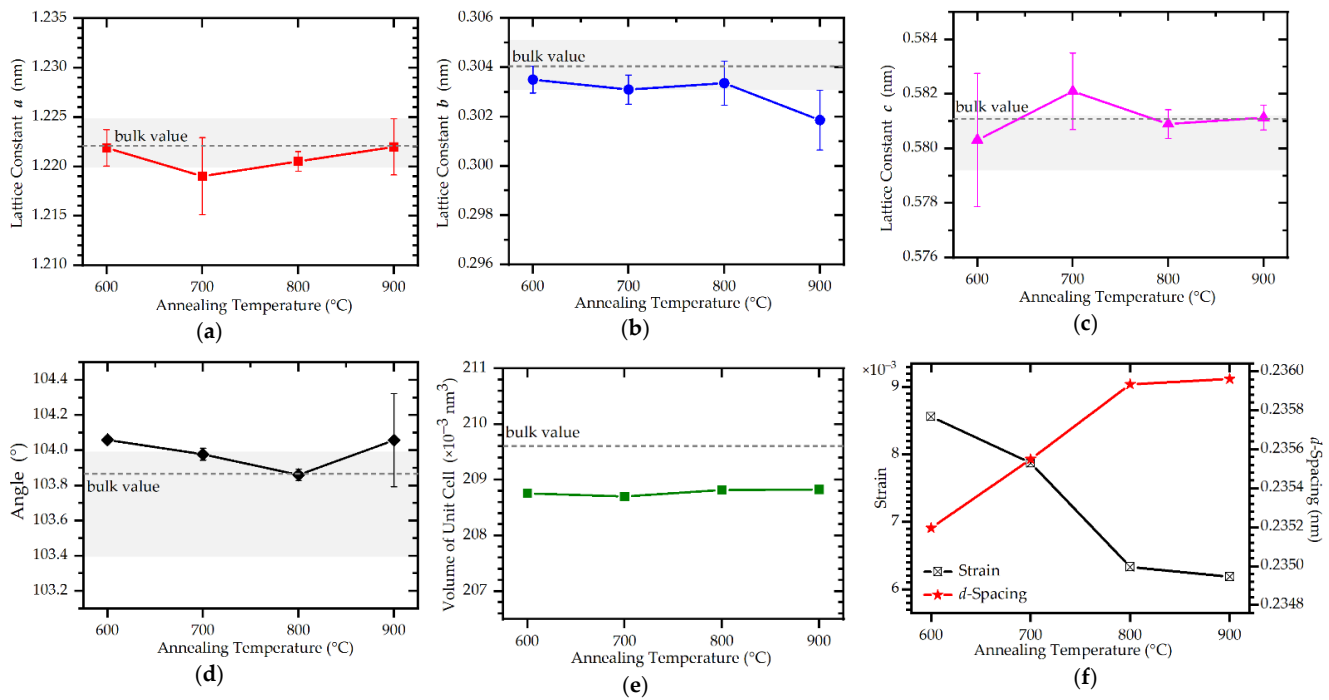


Figure 3. Lattice characteristics of the annealed Ga_2O_3 films with different annealing temperatures of 600, 700, 800, and 900 °C. (a–c) Lattice constants of a , b , and c , respectively. (d) Angle between the a - and c -axes of β . (e) Volume of a unit cell obtained from the expression $V = abc \cdot \sin\beta$, for monoclinic systems. The bulk values of the lattice constants are $a = 1.2222$ nm, $b = 0.3041$ nm, $c = 0.5809$ nm, and $\beta = 103.85^\circ$; therefore, the bulk value of the volume of the unit cell is $V = 209.6265 \times 10^{-3} \text{ nm}^3$ [36]. The range of the reference values of lattice constants was shaded with $a = 1.223 \pm 0.002$ nm, $b = 0.304 \pm 0.001$ nm, $c = 0.580 \pm 0.001$ nm, and $\beta = 103.7 \pm 0.3^\circ$ [1,43,44]. (f) Strain (ϵ) and d -spacing along the (-402) plane.

Figure 3f shows the interplanar distances corresponding to the d -spacings for the monoclinic Ga_2O_3 orientation along the (-402) plane with a change in temperature from 600 to 900 °C. The d -spacing value corresponding to the (-402) plane was calculated using the equation $d_{-402} = \lambda/2\sin\theta$, where λ is the $\text{K}\alpha$ radiation wavelength of Cu ($\lambda = 0.15406$ nm) and θ is the Bragg angle corresponding to the diffraction peak obtained from the XRD data [49]. The d_{-402} value of the annealed Ga_2O_3 films was lower than the bulk value (0.249 nm) because the films were compressively strained within the range of 600–900 °C [50], which was generally attributed to the different equilibrium lattice spacing of the films with the substrate in the much thinner films than the substrate [51]. The d_{-402} values of the annealed Ga_2O_3 films increased from 0.23520 to 0.23596 nm with an increase in temperature from 600 to 900 °C. The release of the compressive strain causes a shifting of the diffraction peak along (-402) towards a lower Bragg angle [39], as shown in Figure 2, which increases the d -spacing in the above equation. The slope of the increase in d_{-402} gradually decreased with the gentle release in the compressive strain at 900 °C. The d -spacing finally approached the more standard value due to the gradual shifting of the diffraction peak along (-402) towards a lower Bragg angle under the same condition, which was possibly due to the

existence of considerable point defects, including oxygen vacancy in the lattice [8,33,52]. It became necessary to examine the XPS analysis results to identify the cause of the rapid decrease in temperature.

To further study the quality of the Ga₂O₃ films, particularly the oxygen vacancies inside the films, the chemical compositions and bonding energies of the films were investigated by XPS at the annealing temperatures of 800 and 900 °C, showing a sharp difference in the lattice characteristics (Figure 2), as shown in Figure 4. All the XPS spectra were deconvoluted using XPSPEAK4.1 software (Washington State University, Pullman, WA, USA). The spectrum of the C 1s peak with a binding energy of 285 eV was used as a reference for data calibration. High-resolution narrow scans were employed to examine the core-level elements, such as Ga 2*p*, Ga 3*d*, and O 1*s*, in the Ga₂O₃ films. The core-level XPS spectra of the annealed Ga₂O₃ film at 800 °C shifted by 0.677–0.870 eV toward a higher binding energy than that at 900 °C. The chemical shift towards higher binding energy without any obvious change in the spectral shape is due to the large electronegativity difference between the coordinating groups. This difference can be attributed to the formation of a large number of crystal defects in the annealed Ga₂O₃ film at 800 °C, which shows the presence of both β-Ga₂O₃ and ε-Ga₂O₃ phases, as observed from the XRD results. The Ga 2*p* doublet was symmetric and narrow at the binding energies of 1118.49 and 1117.76 eV (Ga 2*p*_{3/2}) and 1145.36 and 1144.64 eV (Ga 2*p*_{1/2}) in the annealed Ga₂O₃ films at 800 and 900 °C, respectively, with a spin-orbit splitting (SOS) energy of 26.87 eV, as shown in Figure 4a,d. The small peaks at 1138.37 and 1136.77 eV were loss features between two spin-orbit coupled peaks originating from inelastic interactions between the emerging electrons, which reduced their energy. Because the Ga 2*p* peaks have no appreciable shoulder-like feature, as direct evidence for the gallium interstitials, which also have very high formation energy [53], the origin is deduced to be rather due to oxygen vacancies or others.

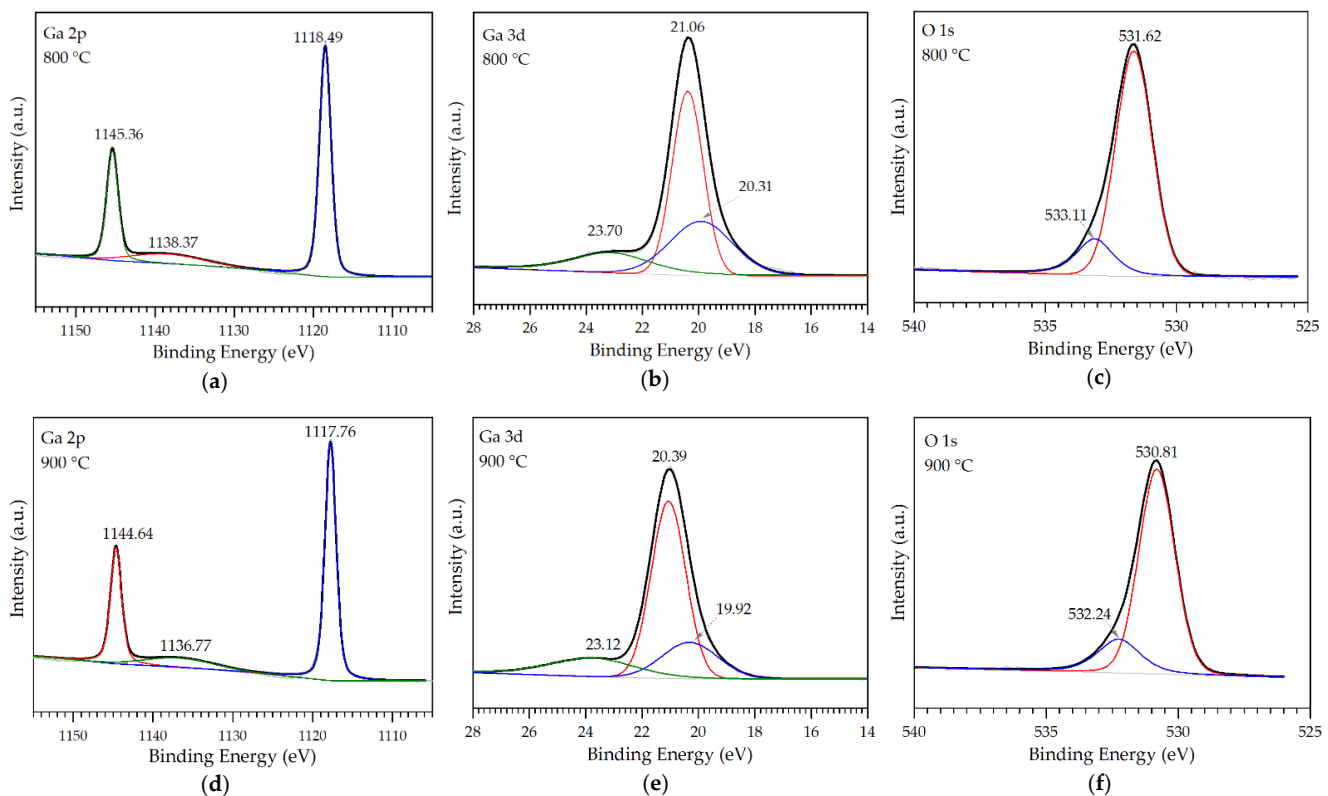


Figure 4. X-ray photoelectron spectra of (a,d) Ga 2*p*_{3/2} (blue) and Ga 2*p*_{1/2} (red) of Ga 2*p*, (b,e) Ga 3*d*_{5/2} (red) and Ga 3*d*_{3/2} (green) of Ga 3*d*, and (c,f) O 1*s* obtained from the annealed Ga₂O₃ films at (a–c) 800 °C and (d–f) 900 °C.

The Ga 3*d* peaks in Figure 4b,e were deconvoluted into two peaks situated at 21.06 and 20.39 eV (Ga 3*d*_{5/2}) and 20.31 and 19.92 eV (Ga 3*d*_{3/2}) for the annealed Ga₂O₃ films at 800 and 900 °C, respectively. This was in addition to the overlapped O 2*s* peaks at 23.70 and 23.12 eV. The Ga 3*d*_{5/2} peaks centered at the high binding energies of 21.06 and 20.39 eV represented the Ga³⁺ oxidation state associated with the Ga–O bond expected in the Ga₂O₃ [54]. The Ga 3*d*_{3/2} peaks at the low binding energies of 20.31 and 19.92 eV may be related to the Ga⁺ or Ga²⁺ oxidation state in the GaO_x bond; this observation suggests either a Ga-rich growth or a presence of oxygen vacancies near the surface.

In Figure 4c,f, each O 1*s* peak in the annealed films at 800 and 900 °C comprised two peaks, O(I) at 531.62 and 530.81 eV, corresponding to the lattice oxygen Ga–O bonds of Ga₂O₃ and O(II) at 533.11 and 532.24 eV, respectively, associated with defected oxygen sub-lattice such as oxygen-related vacancies in the Ga₂O₃ films [55]. However, the area ratio of the O(II) to O 1*s* peaks in the annealed films increased from 11.73% at 800 °C to 17.69% at 900 °C, indicating that the annealed film at 900 °C had a slight increase in the oxygen vacancies. Therefore, it was inferred that prominent defects which resulted in shifting of binding energy at 800 °C are other defects including dislocation rather than the oxygen vacancy, which needs to be investigated more closely in a follow-up study.

TEM was conducted to examine the crystalline quality of the annealed Ga₂O₃ films on the *c*-plane (0001) sapphire substrates at 800 and 900 °C, which were the changed conditions in the crystalline state at all annealing temperatures. Figure 5 shows the high-resolution TEM images, SAED patterns, and inverse fast Fourier transform (IFFT) images of the films. Figure 5a–c show the TEM image, SAED pattern, and inverse Fourier transform (IFFT) image, respectively, of the annealed Ga₂O₃ film at 800 °C. Three nanocrystalline planes (systems of parallel equidistant lines) with interplanar distances of 0.23588, 0.14820, and 0.46930 nm corresponding to β-Ga₂O₃ were observed [56]. The TEM image of the films at 800 °C shows Moiré fringes due to several minute β-Ga₂O₃ (−402) nanocrystals with a pseudomorphic coherence for (−603) and (−201) orientations, which may have originated from the partial symmetry mismatch between the monoclinic β-Ga₂O₃ and hexagonal ε-Ga₂O₃ [57–59]. Notably, the Moiré fringes did not necessarily appear at high dislocation densities in the films [60]. Detailed information on the lattice dislocation structure of the nanocrystals in the film at 800 °C was obtained by the IFFT of the TEM image. The IFFT image, obtained from the center of the TEM image in Figure 5a, shows linear defects, including an edge dislocation (T-shaped symbol) and screw dislocations (red-dashed rectangular frames) [61].

The TEM image in Figure 5d shows that the orientation of the annealed Ga₂O₃ film at 900 °C improved despite the remaining dislocations, which comprised regions with a better atomic arrangement, showing an aligned arrangement sloping with distinct angles and interplanar distances of upward to the left with 0.23529 nm. These correspond to the *d*-spacing of the monoclinic β-Ga₂O₃ (−402) plane with similar XRD results in Figure 3f. Figure 5d shows that the annealed Ga₂O₃ films at 900 °C exhibit a polycrystalline nature with β-Ga₂O₃ (−402) texture-dominated crystal films, correlating with the XRD results. As shown in the SAED pattern, diffraction spots and dispersive diffraction rings were observed, owing to the presence of polycrystalline components in the films. The IFFT image obtained from the center of the TEM image in Figure 5d shows ordered lattice fringes with the same *d*-spacings, as shown in Figure 5f. This confirms that linear defects, such as dislocations and boundaries, as shown in Figure 5c, decreased. As expected for the annealed Ga₂O₃ film at 900 °C with the relaxed strains, it can achieve significantly reduced defects and relatively clear and uniform β-Ga₂O₃, although they were not perfect because of the unintended occurrence of point defects at 900 °C.

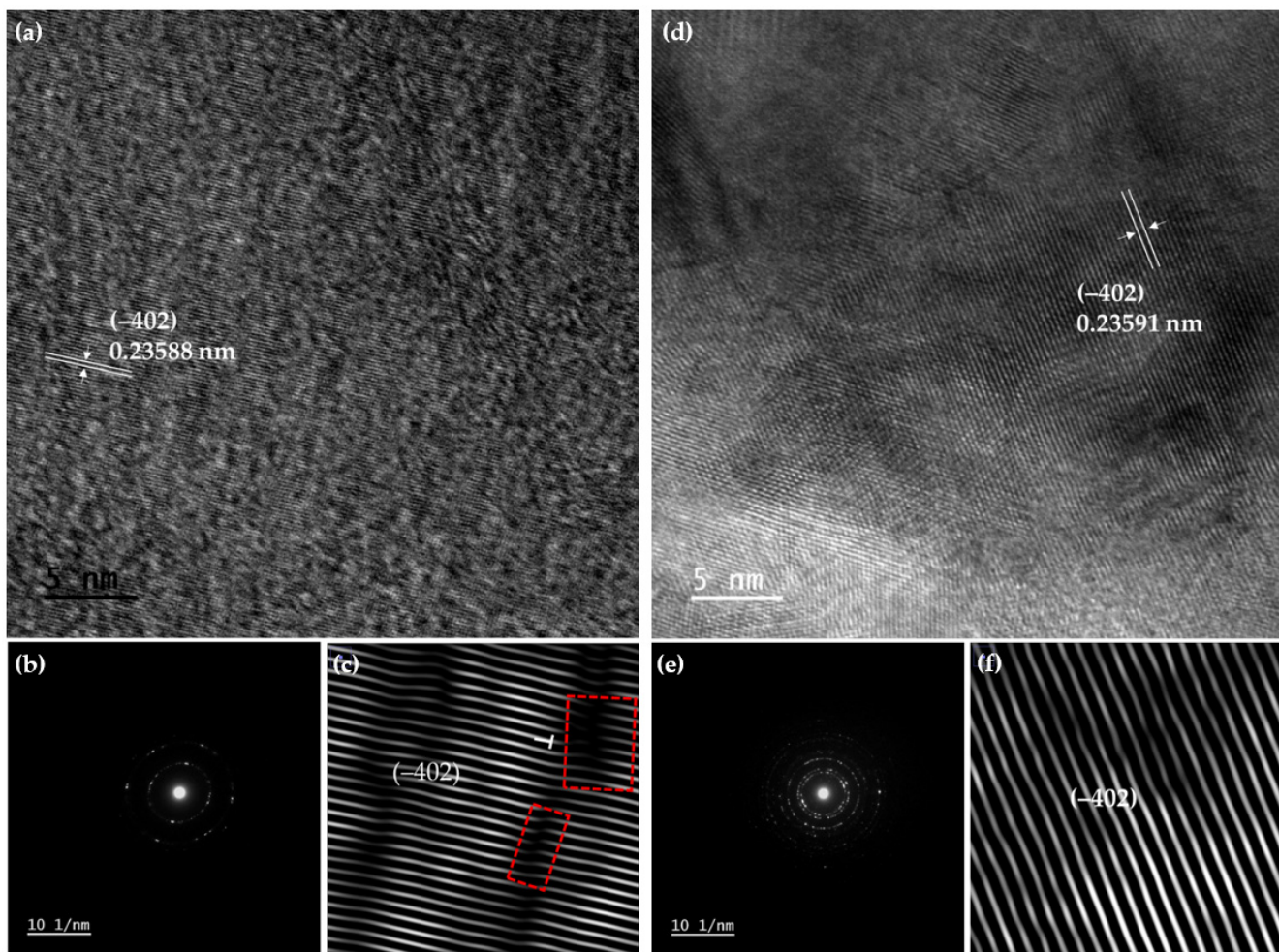


Figure 5. (a,d) Transmission electron microscopy (TEM) images, (b,e) selected area electron diffraction (SAED) patterns, and (c,f) inverse fast Fourier transform (IFFT) images of the annealed β - Ga_2O_3 films at the annealing temperatures of (a–c) 800 °C and (d–f) 900 °C.

4. Conclusions

Improved crystalline quality β - Ga_2O_3 films on c-plane sapphire substrates were fabricated by RF magnetron sputtering deposition followed by RTA at 900 °C for 45 min. The amorphous nature of the Ga_2O_3 films was observed in the as-deposited and annealed films at a low temperature of 500 °C; a mixture of ϵ - and β -phases was observed within the range of 600–800 °C, whereas only the β -phase appeared with a crystallite size of 26.02 nm at 900 °C. The d-spacing decreased and approached the standard value when the strain was consistently relaxed with an increase in the annealing temperature to 900 °C. Although the dislocation density in the annealed Ga_2O_3 films was reduced at 900 °C, a clear and uniform orientation was not achieved, and the oxygen vacancy concentration increased in the film at that annealing temperature. Nevertheless, a better polycrystalline nature with a dominant β - Ga_2O_3 (-402)-preferred crystal film was achieved from the annealed Ga_2O_3 film at 900 °C. A follow-up study to grow a β - Ga_2O_3 single crystal on the buffer layer of the c-plane sapphire substrate with improved crystal quality under the process conditions for mass production and confirm its characteristics will be required.

Supplementary Materials: The following supporting information can be downloaded at: <https://www.mdpi.com/article/10.3390/coatings12020140/s1>, Figure S1: Cross-sectional field emission scanning electron microscope (FESEM) images of (a) as-deposited and annealed Ga_2O_3 films at different post-annealing temperatures: (b) 500, (c) 600, (d) 700, (e) 800, and (f) 900 °C.

Author Contributions: Conceptualization, S.P., S.K. and N.-H.K.; methodology, S.P. and N.-H.K.; investigation, S.P., S.K. and N.-H.K.; data curation, S.P.; writing—original draft preparation, S.P., S.K. and N.-H.K.; writing—review and editing, S.K. and N.-H.K.; supervision, N.-H.K.; project administration, N.-H.K.; funding acquisition, N.-H.K. All authors have read and agreed to the published version of the manuscript.

Funding: This study was supported by a research fund from Chosun University, 2021.

Institutional Review Board Statement: Not applicable.

Informed Consent Statement: Not applicable.

Data Availability Statement: Data are contained within the article or Supplementary Materials.

Conflicts of Interest: The authors declare no conflict of interest. The founding sponsors had no role in the design of the study; in the collection, analyses, or interpretation of data; in the writing of the manuscript, or in the decision to publish the results.

References

1. Saikumar, A.K.; Nehate, S.D.; Sundaram, K.B. Review—RF Sputtered Films of Ga₂O₃. *ECS J. Solid State Sci. Technol.* **2019**, *8*, Q3064–Q3078. [[CrossRef](#)]
2. Wu, J.; Mi, W.; Yang, Z.; Chen, Y.; Li, C.; Zhao, J.; Zhang, K.; Zhang, X.; Luan, C. Influence of annealing on the structural and optical properties of gallium oxide films deposited on c-sapphire substrate. *Vacuum* **2019**, *167*, 6–9. [[CrossRef](#)]
3. Bosi, M.; Mazzolini, P.; Seravalli, L.; Fornari, R. Ga₂O₃ polymorphs: Tailoring the epitaxial growth conditions. *J. Mater. Chem. C* **2020**, *8*, 10975–10992. [[CrossRef](#)]
4. Xue, H.; He, Q.; Jian, G.; Long, S.; Pang, T.; Liu, M. An Overview of the Ultrawide Bandgap Ga₂O₃ Semiconductor-Based Schottky Barrier Diode for Power Electronics Application. *Nanoscale Res. Lett.* **2018**, *13*, 290. [[CrossRef](#)] [[PubMed](#)]
5. Li, M.Q.; Yang, N.; Wang, G.G.; Zhang, H.Y.; Han, J.C. Highly preferred orientation of Ga₂O₃ films sputtered on SiC substrates for deep UV photodetector application. *Appl. Surf. Sci.* **2019**, *471*, 694–702. [[CrossRef](#)]
6. Liu, X.; Liu, Q.; Zhao, B.; Ren, Y.; Tao, B.W.; Zhang, W.L. Comparison of β-Ga₂O₃ thin films grown on r-plane and c-plane sapphire substrates. *Vacuum* **2020**, *178*, 109435. [[CrossRef](#)]
7. Nakagomi, S.; Kokubun, Y. Crystal orientation of β-Ga₂O₃ thin films formed on c-plane and a-plane sapphire substrate. *J. Cryst. Growth* **2012**, *349*, 12–18. [[CrossRef](#)]
8. Ghosh, S.; Srivastava, H.; Rao, P.N.; Nand, M.; Tiwari, P.; Srivastava, A.K.; Jha, S.N.; Rai, S.K.; Singh, S.D.; Ganguli, T. Investigations on epitaxy and lattice distortion of sputter deposited β-Ga₂O₃ layers on GaN templates. *Semicond. Sci. Technol.* **2020**, *35*, 085024. [[CrossRef](#)]
9. Li, W.; Zhang, X.; Meng, R.; Yan, J.; Wang, J.; Li, J.; Wei, T. Epitaxy of III-Nitrides on β-Ga₂O₃ and Its Vertical Structure LEDs. *Micromachines* **2019**, *10*, 322. [[CrossRef](#)]
10. An, Y.; Daiz, L.; Wuy, Y.; Wuy, B.; Zhaoy, Y.; Liuy, T.; Haoy, H.; Liy, Z.; Niuz, G.; Zhangy, J.; et al. Epitaxial growth of β-Ga₂O₃ thin films on Ga₂O₃ and Al₂O₃ substrates by using pulsed laser deposition. *J. Adv. Dielectr.* **2019**, *9*, 1950032. [[CrossRef](#)]
11. Son, H.; Choi, Y.; Hong, S.-K.; Park, J.-H.; Jeon, D.-W. Reduction of dislocations in α-Ga₂O₃ epilayers grown by halide vapor-phase epitaxy on a conical frustum-patterned sapphire substrate. *IUCrJ* **2021**, *8*, 462–467. [[CrossRef](#)] [[PubMed](#)]
12. Arata, Y.; Nishinaka, H.; Tahara, D.; Yoshimoto, M. Heteroepitaxial growth of single-phase ε-Ga₂O₃ thin films on c-plane sapphire by mist chemical vapor deposition using a NiO buffer layer. *CrystEngComm* **2018**, *20*, 6236–6242. [[CrossRef](#)]
13. Kukushkin, S.A.; Osipov, A.V.; Bessolov, V.N.; Medvedev, B.K.; Nevolin, V.K.; Tcarik, K.A. Substrates for epitaxy of gallium nitride: New materials and techniques. *Rev. Adv. Mater. Sci.* **2008**, *17*, 1–32.
14. Nishinaka, H.; Tahara, D.; Morimoto, S.; Yoshimoto, M. Epitaxial growth of α-Ga₂O₃ thin films on a-, m-, and r-plane sapphire substrates by mist chemical vapor deposition using α-Fe₂O₃ buffer layers. *Mater. Lett.* **2017**, *205*, 28–31. [[CrossRef](#)]
15. Jinno, R.; Uchida, T.; Kaneko, K.; Fujita, S. Reduction in edge dislocation density in corundum-structured α-Ga₂O₃ layers on sapphire substrates with quasi-graded α-(Al,Ga)₂O₃ buffer layers. *Appl. Phys. Express* **2016**, *9*, 071101. [[CrossRef](#)]
16. Oda, M.; Kaneko, K.; Fujita, S.; Hitora, T. Crack-free thick (>5 μm) α-Ga₂O₃ films on sapphire substrates with α-(Al,Ga)₂O₃ buffer layers. *Jpn. J. Appl. Phys.* **2016**, *55*, 1202B4. [[CrossRef](#)]
17. Ngo, T.S.; Le, D.D.; Lee, J.; Hong, S.-K.; Ha, J.-S.; Lee, W.-S.; Moon, Y.-B. Investigation of defect structure in homoepitaxial (-201) β-Ga₂O₃ layers prepared by plasma-assisted molecular beam epitaxy. *J. Alloys Compd.* **2020**, *834*, 155027. [[CrossRef](#)]
18. Liao, Y.; Jiao, S.; Li, S.; Wang, J.; Wang, D.; Gao, S.; Yu, Q.; Li, H. Effect of deposition pressure on the structural and optical properties of Ga₂O₃ films obtained by thermal post-crystallization. *CrystEngComm* **2018**, *20*, 133–139. [[CrossRef](#)]
19. Dong, L.; Jia, R.; Xin, B.; Zhang, Y. Effects of post-annealing temperature and oxygen concentration during sputtering on the structural and optical properties of β-Ga₂O₃ films. *J. Vac. Sci. Technol. A-Vac. Surf. Films* **2016**, *34*, 060602. [[CrossRef](#)]
20. Meng, Y.; Gao, Y.; Chen, K.; Lu, J.; Xian, F.; Xu, L.; Zheng, G.; Kuang, W.; Cao, Z. Annealing induced phase transition and optical properties of Ga₂O₃ thin films synthesized by sputtering technique. *Optik* **2021**, *244*, 167515. [[CrossRef](#)]

21. Kim, S.; Kim, N.-H. Impurity Phases and Optoelectronic Properties of CuSbSe₂ Thin Films Prepared by Cosputtering Process for Absorber Layer in Solar Cells. *Coatings* **2020**, *10*, 1209. [[CrossRef](#)]
22. Wang, R.X.; Beling, C.D.; Fung, S.; Djurišić, A.B.; Ling, C.C.; Kwong, C.; Li, S. Influence of annealing temperature and environment on the properties of indium tin oxide thin films. *J. Phys. D-Appl. Phys.* **2005**, *38*, 2000–2005. [[CrossRef](#)]
23. Lee, J.; Kim, H.; Gautam, L.; He, K.; Hu, X.; Dravid, V.P.; Razeghi, M. Study of phase transition in MOCVD grown Ga₂O₃ from κ to β phase by ex situ and in situ annealing. *Photonics* **2021**, *8*, 17. [[CrossRef](#)]
24. Yao, Y.; Okur, S.; Lyle, L.A.M.; Tompa, G.S.; Salagaj, T.; Sbrockey, N.; Davis, R.F.; Porter, L.M. Growth and characterization of α -, β -, and ϵ -phases of Ga₂O₃ using MOCVD and HVPE techniques. *Mater. Res. Lett.* **2018**, *6*, 268–275. [[CrossRef](#)]
25. Boschi, F.; Bosi, M.; Berzina, T.; Buffagni, E.; Ferrari, C.; Fornari, R. Hetero-epitaxy of ϵ -Ga₂O₃ layers by MOCVD and ALD. *J. Cryst. Growth* **2016**, *443*, 25–30. [[CrossRef](#)]
26. Hsu, C.-H.; Geng, X.-P.; Wu, W.-Y.; Zhao, M.-J.; Zhang, X.-Y.; Huang, P.-H.; Lien, S.-Y. Air Annealing Effect on Oxygen Vacancy Defects in Al-doped ZnO Films Grown by High-Speed Atmospheric Atomic Layer Deposition. *Molecules* **2020**, *25*, 5043. [[CrossRef](#)]
27. Li, S.; Jiao, S.; Wang, D.; Gao, S.; Wang, J. The influence of sputtering power on the structural, morphological and optical properties of β -Ga₂O₃ thin films. *J. Alloys Compd.* **2018**, *753*, 186–191. [[CrossRef](#)]
28. Oshima, T.; Okuno, T.; Fujita, S. Ga₂O₃ Thin Film Growth on c-Plane Sapphire Substrates by Molecular Beam Epitaxy for Deep-Ultraviolet Photodetectors. *Jpn. J. Appl. Phys.* **2007**, *46*, 7217–7220. [[CrossRef](#)]
29. Xu, Y.; Park, J.-H.; Yao, Z.; Wolverson, C.; Razeghi, M.; Wu, J.; Dravid, V.P. Strain-Induced Metastable Phase Stabilization in Ga₂O₃ Thin Films. *ACS Appl. Mater. Interfaces* **2019**, *11*, 5536–5543. [[CrossRef](#)]
30. Tak, B.R.; Kumar, S.; Kapoor, A.K.; Wang, D.; Li, X.; Sun, H.; Singh, R. Recent advances in the growth of gallium oxide thin films employing various growth techniques-A review. *J. Phys. D Appl. Phys.* **2021**, *54*, 453002. [[CrossRef](#)]
31. Ghose, S.; Rahman, S.; Hong, L.; Rojas-Ramirez, J.S.; Jin, H.; Park, K.; Klie, R.; Droopad, R. Growth and characterization of β -Ga₂O₃ thin films by molecular beam epitaxy for deep-UV photodetectors. *J. Appl. Phys.* **2017**, *122*, 095302. [[CrossRef](#)]
32. Jiao, S.; Lu, H.; Wang, X.; Nie, Y.; Wang, D.; Gao, S.; Wang, J. The Structural and Photoelectrical Properties of Gallium Oxide Thin Film Grown by Radio Frequency Magnetron Sputtering. *ECS J. Solid State Sci. Technol.* **2019**, *8*, Q3086–Q3090. [[CrossRef](#)]
33. Lv, Y.; Ma, J.; Mi, W.; Luan, C.; Zhu, Z.; Xiao, H. Characterization of β -Ga₂O₃ thin films on sapphire (0001) using metal-organic chemical vapor deposition technique. *Vacuum* **2012**, *86*, 1850–1854. [[CrossRef](#)]
34. Feng, Z.; Huang, L.; Feng, Q.; Li, X.; Zhang, H.; Tang, W.; Zhang, J.; Hao, Y. Influence of annealing atmosphere on the performance of a β -Ga₂O₃ thin film and photodetector. *Opt. Mater. Express* **2018**, *8*, 2229–2237. [[CrossRef](#)]
35. Patterson, A.L. The Scherrer formula for X-ray particle size determination. *Phys. Rev.* **1939**, *56*, 978–982. [[CrossRef](#)]
36. Williamson, G.K.; Hall, W.H. X-ray line broadening from filed aluminium and wolfram. *Acta Metall. Mater.* **1953**, *1*, 22–31. [[CrossRef](#)]
37. Joshi, G.; Chauhan, Y.S.; Verma, A. Temperature Dependence of β -Ga₂O₃ Heteroepitaxy on c-plane Sapphire using Low Pressure Chemical Vapor Deposition. *J. Alloys Compd.* **2021**, *883*, 160799. [[CrossRef](#)]
38. Mote, V.D.; Purushotham, Y.; Dole, B.N. Williamson-Hall analysis in estimation of lattice strain in nanometer-sized ZnO particles. *J. Theor. Appl. Phys.* **2012**, *6*, 6. [[CrossRef](#)]
39. Kumar, S.; Asokan, K.; Singh, R.K.; Chatterjee, S.; Kanjilal, D.; Ghosh, A.K. Investigations on structural and optical properties of ZnO and ZnO: Co nanoparticles under dense electronic excitations. *RSC Adv.* **2014**, *4*, 62123–62131. [[CrossRef](#)]
40. Boonlakhorn, J.; Prachamon, J.; Manyam, J.; Kongsuk, S.; Thongbai, P.; Srepusharawoot, P. Colossal dielectric permittivity, reduced loss tangent and the microstructure of Ca_{1-x}Cd_xCu₃Ti₄O_{12-2y}F_{2y} ceramics. *RSC Adv.* **2021**, *11*, 16396–16403. [[CrossRef](#)]
41. Negi, J.; Panwar, N.S. Structural and electrical properties of lead-free Na_{0.685}K_{0.315}Nb_{1-y}Ta_yO₃ (0 ≤ y ≤ 0.05) ceramics. *J. Phys. Chem. Solids* **2021**, *151*, 109853. [[CrossRef](#)]
42. Bel, A.M.T.; Clegg, F.; Henderson, C.M.B. Monoclinic–orthorhombic first-order phase transition in K₂ZnSi₅O₁₂ leucite analogue; transition mechanism and spontaneous strain analysis. *Mineral. Mag.* **2021**, *85*, 1–20. [[CrossRef](#)]
43. Geller, S. Crystal Structure of β -Ga₂O₃. *J. Chem. Phys.* **1960**, *33*, 676. [[CrossRef](#)]
44. McCluskey, M.S. Point defects in Ga₂O₃. *J. Appl. Phys.* **2020**, *127*, 101101. [[CrossRef](#)]
45. Marai, A.B.; Belgacem, J.B.; Ayadi, J.B.; Djessas, K.; Alaya, S. Structural and optical properties of CuIn_{1-x}Ga_xSe₂ nanoparticles synthesized by solvothermal route. *J. Alloys Compd.* **2016**, *658*, 961–966. [[CrossRef](#)]
46. Goh, K.H.; Haseeb, A.S.M.A.; Wong, Y.H. Physical and electrical properties of thermal oxidized Sm₂O₃ gate oxide thin film on Si substrate: Influence of oxidation durations. *Thin Solid Films* **2016**, *606*, 80–86. [[CrossRef](#)]
47. Rabiei, M.; Palevicius, A.; Monshi, A.; Nasiri, S.; Vilkauskas, A.; Janusas, G. Comparing Methods for Calculating Nano Crystal Size of Natural Hydroxyapatite Using X-ray Diffraction. *Nanomaterials* **2020**, *10*, 1627. [[CrossRef](#)] [[PubMed](#)]
48. Cora, I.; Mezzadri, F.; Boschi, F.; Bosi, M.; Čaplovičová, M.; Calestani, G.; Dódony, I.; Pécz, B.; Fornari, R. The real structure of ϵ -Ga₂O₃ and its relation to κ -phase. *CrystEngComm* **2017**, *19*, 1509–1516. [[CrossRef](#)]
49. Shokeen, P.; Jain, A.; Kapoor, A.; Gupta, V. Thickness and Annealing Effects on the Particle Size of PLD Grown Ag Nanofilms. *Plasmonics* **2016**, *11*, 669–675. [[CrossRef](#)]
50. Chen, Z.; Wang, X.; Noda, S.; Saito, K.; Tanaka, T.; Nishio, M.; Arita, M.; Guo, Q. Effects of dopant contents on structural, morphological and optical properties of Er doped Ga₂O₃ films. *Superlattices Microstruct.* **2016**, *90*, 207–214. [[CrossRef](#)]
51. Cammarata, R.C. Stresses in thin films. In *Surface Modification and Mechanisms: Friction, Stress, and Reaction Engineering*, 1st ed.; Totten, G.E., Liang, H., Eds.; Marcel Dekker Inc.: New York, NY, USA, 2005; pp. 20–35.

52. Zhao, M.-J.; Sun, Z.-T.; Zhang, Z.-X.; Geng, X.-P.; Wu, W.-Y.; Lien, S.-Y.; Zhu, W.-Z. Suppression of Oxygen Vacancy Defects in sALD-ZnO Films Annealed in Different Conditions. *Materials* **2020**, *13*, 3910. [[CrossRef](#)] [[PubMed](#)]
53. Chikoidze, E.; Rogers, D.J.; Teherani, F.H.; Rubio, C.; Sauthier, G.; Von Bardeleben, H.J.; Tchelidze, T.; Ton-That, C.; Fellous, A.; Bove, P.; et al. Puzzling robust 2D metallic conductivity in undoped β -Ga₂O₃ thin films. *Mater. Today Phys.* **2019**, *8*, 10–17. [[CrossRef](#)]
54. Chen, J.X.; Li, X.X.; Ma, H.P.; Huang, W.; Ji, Z.G.; Xia, C.; Lu, H.L.; Zhang, D.W. Investigation of the Mechanism for Ohmic Contact Formation in Ti/Al/Ni/Au Contacts to β -Ga₂O₃ Nanobelt Field-Effect Transistors. *ACS Appl. Mater. Interfaces* **2019**, *11*, 32127–32134. [[CrossRef](#)] [[PubMed](#)]
55. Rafique, S.; Han, L.; Zhao, H. Thermal annealing effect on β -Ga₂O₃ thin film solar blind photodetector heteroepitaxially grown on sapphire substrate. *Phys. Status Solidi A-Appl. Mater.* **2017**, *214*, 1700063. [[CrossRef](#)]
56. Rajamani, S.; Arora, K.; Belov, A.; Korolev, D.; Nikolskaya, A.; Usov, Y.; Pavlov, D.; Mikhaylov, A.; Tetelbaum, D.; Kumar, M.; et al. Enhanced Solar-Blind Photodetection Performance of Encapsulated Ga₂O₃ Nanocrystals in Al₂O₃ Matrix. *IEEE Sens. J.* **2018**, *18*, 4046–4052. [[CrossRef](#)]
57. Zhuo, Y.; Chen, Z.; Tu, W.; Ma, X.; Pei, Y.; Wang, G. β -Ga₂O₃ versus ϵ -Ga₂O₃: Control of the crystal phase composition of gallium oxide thin film prepared by metal-organic chemical vapor deposition. *Appl. Surf. Sci.* **2017**, *420*, 802–807. [[CrossRef](#)]
58. Schewski, R.; Wagner, G.; Baldini, M.; Gogova, D.; Galazka, Z.; Schulz, T.; Remmele, T.; Markurt, T.; Von Wenckstern, H.; Grundmann, M.; et al. Epitaxial stabilization of pseudomorphic α -Ga₂O₃ on sapphire (0001). *Appl. Phys. Express* **2014**, *8*, 011101. [[CrossRef](#)]
59. Prokes, S.M.; Katz, M.B.; Twigg, M.E. Growth of crystalline Al₂O₃ via thermal atomic layer deposition: Nanomaterial phase stabilization. *APL Mater.* **2014**, *2*, 032105. [[CrossRef](#)]
60. Rentenberger, C.; Waitz, T.; Karnthaler, H.P. HRTEM analysis of nanostructured alloys processed by severe plastic deformation. *Scr. Mater.* **2004**, *51*, 789–794. [[CrossRef](#)]
61. Zhang, Z.; Ódor, É.; Farkas, D.; Jóni, B.; Ribárik, G.; Tichy, G.; Nandam, S.H.; Ivanisenko, J.; Preuss, M.; Ungár, T. Dislocations in grain boundary regions: The origin of heterogeneous microstrains in nanocrystalline materials. *Metall. Mater. Trans. A-Phys. Metall. Mater. Sci.* **2020**, *51*, 513–530. [[CrossRef](#)]